

A Novel Vibration-based Structure Health Monitoring Approach for the Shallow Buried Tunnel

Biao Zhou^{1,2,3}, Xiong yao Xie^{1,2}, Yeong Bin Yang⁴ and Jing Cai Jiang³

Abstract: The vibration-based SHM (Structure Health Monitoring) system has been successfully used in bridge and other surface civil infrastructure. However, its application in operation tunnels remains a big challenge. The reasons are discussed in this paper by comparing the vibration characteristics of the free tunnel structure and tunnel-soil coupled system. It is revealed that all the correlation characteristics of the free tunnel FRFs (Frequency Response Function spectrum) will vanish and be replaced by a coupled resonance frequency when the tunnel is surrounded by soil. The above statement is validated by field measurements. Moreover, the origin of this phenomenon is investigated by dispersion analysis based on a novel simulation model termed as TTMM (Timoshenko beam-Transfer Matrix Method). It is proved that the coupled resonance frequency occurs at the intersection of soil and free tunnel flexible wave mode dispersion curves. A simplified method is developed to determine the relationship between the tunnel Young's modulus and the coupled resonance frequency, which can be employed as an index for quantifying the tunnel global stiffness.

Keywords: Structure Health Monitoring, Timoshenko beam-Transfer Matrix Method, Frequency Response Function spectrum, free tunnel, tunnel-soil coupled system

1 Introduction

After years of operation, a number of problems were found in the tunnels of Shanghai metro line. Among them, leakage, segment crack and concrete spalling, longitudinal settlement, high rate of settlement are identified as the most common ones [Li, Wang, Yan (2008)]. With increasing awareness of metro's economic and social effects, the management team and researchers have been planning to introduce

¹ Key Laboratory of Geotechnical & Underground Engineering, Ministry of Education, Tongji University, Shanghai 200092, China

² Department of Geotechnical Engineering, Tongji University, Shanghai 200092, China

³ Department of civil Engineering, Tokushima University, Tokushima 770-8501, Japan

⁴ Department of civil Engineering, National Taiwan University, Taipei 10617, Taiwan, R.O. China

the Structure Health Monitoring (SHM) system into the tunnel monitoring system. This technology has been successfully used in monitoring bridge and other civil infrastructures [Aktan, Catbas and Grimmelsman (2003); Peter, Flatau and Liu (2003)], and relevant vibration-based methods are employed to determine the structure service condition. The vibration-based methods apply damage-induced changes to the dynamic properties of a structure to detect, locate, and sometimes quantify the extent of damage. [Carden and Paul (2004)] provided a review of the above methods and made classification of the prevailing methods in this field. It mainly includes Natural Frequency Based Methods, FRF Based Methods, Mode Shape Based Methods, Mode Shape Curvature/Strain Mode Shape Based Methods, Dynamically Measured Flexibility Based Methods, Matrix Update Based Methods, Non-linear Methods, Neural Network Based Methods, etc.

All these methods are developed and based on the consideration of structure vibration characteristics. Therefore, it is important to analyze these vibration characteristics before applying SHM to operation tunnels. In practice, an operational tunnel can be analogous to a long extended tunnel-soil coupled system, and the soil properties will greatly change the vibration propagation in the tunnel structure. Thus, it will bring big challenge to the application of SHM. The correlation analysis of above issues requires application of realistic methods. One of the most important pioneering work employed to simulate the infinite extend periodic structure vibration is the periodic solution approach. Such approaches were first proposed by [Hwang and Lysmer (1981)] and [Clouteau, Elhabre and Aubry (2000)] in studying the response of an underground structure to seismic waves propagation.

In Hwang and Lysmer's work, by assuming constant material and geometric properties, only the profile of the 2D cross-section plane normal to the long infinite extended direction needs be considered. The effect from this direction can be calculated by Fourier transformation. Later, for dealing with the ground vibrations induced by moving loads, [Yang and Huang (2001, 2008)] extended this idea by combining with FE-IFE method and termed as 2.5D method. An approach based on similar concept was also introduced in a computationally efficient model called Pipe-in-Pipe (PIP) for calculating the vibration from underground railways ([Forrest and Hunt (2006)] and [Hussein and Hunt (2007)]) where tunnel structure and its surrounding infinite soil were modelled as two concentric pipes. The inner pipe representing the tunnel structure was modelled based on the thin shell theory. The outer pipe representing the infinite soil was modelled as a 3D homogeneous, isotropic elastic thick-walled cylinder, with its inner diameter set equal to the diameter of the tunnel and its outer diameter set to infinity.

Similarly, [Clouteau, Elhabre and Aubry (2000)] assumed that the structure had periodicity along the infinite extended direction, and only a reference cell normal

to the long infinite extended direction needed be considered. And the effect from this direction could be considered by Floquet transformation. Based on the above method, the FE-BE coupled model was combined by [Gupta, Degrande and Lombaert (2009)] to compute the wave field radiated into the soil of a track-tunnel-soil interaction problem in the frequency-wavenumber domain, in which the boundary elements were used for the soil and finite elements for the tunnel.

All the aforementioned approaches have been successfully applied in simulating the vibration propagation in the tunnel-soil coupled system. In this work, by combining with the periodic approach mentioned above, a thin wall cylinder shell theory and the FE-IFE method will be employed to calculate the FRFs (Frequency Response Function spectrum) and vibration characteristics of the free tunnel and tunnel-soil coupled system, respectively. It is found that the resonance frequencies of the free tunnel can be identified from the peaks of driving point (the point where load is applied) FRFs. Then, based on the 2.5D FE-IFE method, a MATLAB toolbox is developed to simulate the dynamic response of the tunnel-soil coupled system. For the case of shallow-buried tunnel, with harmonic loads with different frequency applied at the tunnel invert, the driving point displacement FRFs is greatly different from that of free tunnel. A coupled resonance frequency is found at low frequency (<5Hz), the rest of the FRFs curve is smooth and no marked peaks appeared. The simulation results are validated by the field measurement and the details will be given in section 4. The aforementioned findings show that it is not feasible to obtain any useful information related to the tunnel nature frequency and modal characteristics from the tunnel dynamic responses. And that will be a big challenge for the conventional vibration-based SHM method mentioned above.

In section 3 a novel approach is developed based on the coupled resonance frequency found at tunnel displacement FRFs. The origin of the resonance frequency is exploited by performing dispersion analysis for the free tunnel and soil layer, respectively. It is found that the first propagation wave mode of the soil layer underneath the tunnel is approximately a straight line and intersect only with the tunnel first flexible wave mode at low frequency range. The cross point correspond exactly to the coupled resonance frequency. Meanwhile, it also explains why the rest of displacement FRFs corresponds to a smooth curve. In such a case, by assuming that the soil properties are constant during the tunnel operation period, the changes in resonance frequency indicate the variation of the tunnel physical properties. For the tunnel flexible wave mode dispersion curve can be modelled by a Timoshenko beam, a novel approach permitting to determine the relationship between the coupled resonance frequency and tunnel Young's modulus, which can be regarded as an index to judge the tunnel service condition.

2 Challenges of SHM used in operation tunnel

Based on the periodic solution and taking the Shanghai metro line 11 as a background, the main purpose of this section is to investigate and compare the vibration characteristics of the free tunnel and tunnel-soil coupled system. Within frequency range of interest from 0 to 100Hz, several resonance frequencies can be found from the free tunnel displacement FRFs. However, once the tunnel is coupled with soil layer, only one coupled resonance frequency with totally different frequency can be found. The vastly different vibration characteristics will bring big challenge for the conventional vibration-based SHM method.

2.1 Basic theory of periodic approach and background

By assuming constant material and geometric properties along the infinite extended direction z , as shown in Fig.6, the function of the loading applied at the 2D x - y plane normal to the z direction are harmonic both in time and z direction, as follows:

$$\tilde{\mathbf{f}} = \tilde{\mathbf{Q}}(x, y)e^{i(\beta z + \omega t)}, \tilde{\mathbf{Q}}(x, y) = [\tilde{Q}_x(x, y), \tilde{Q}_y(x, y), \tilde{Q}_z(x, y)]^T \quad (1)$$

where $\mathbf{Q}(x, y)$ represents the influence function of the applied loads at x, y, z direction in x - y plane and can be expressed as $Q_x(x, y), Q_y(x, y), Q_z(x, y)$, respectively.

If the response is linear, the displacement field can be similarly expressed by harmonic its components:

$$\tilde{\mathbf{D}} = \tilde{\mathbf{U}}(x, y)e^{i(\beta z + \omega t)}, \tilde{\mathbf{U}}(x, y) = [\tilde{u}(x, y) \quad \tilde{v}(x, y) \quad \tilde{w}(x, y)]^T \quad (2)$$

where $\mathbf{U}(x, y)$ is the displacement response which consists of $u(x, y), v(x, y)$ and $w(x, y)$ representing the displacement at x, y, z direction in x - y plane, respectively.

The tilde on the uppercase coefficients $\mathbf{Q}(x, y)$ and $\mathbf{U}(x, y)$ indicates that they are in the frequency-wavenumber domain. The final steady-state response in time domain can be obtained by superimposing the response $\mathbf{U}(x, y)$ generated by each of the harmonic and wavenumber components β and ω . It can be expressed as:

$$\mathbf{U}(x, y) = \frac{1}{4\pi^2} \int_{-\infty}^{\infty} \int_{-\infty}^{\infty} \tilde{\mathbf{U}}(x, y)e^{i(\beta z + \omega t)} d\omega d\beta, \tilde{\mathbf{U}} = [\tilde{u}(x, y) \quad \tilde{v}(x, y) \quad \tilde{w}(x, y)]^T \quad (3)$$

If the applied load with a self-oscillation frequency ω , Eq. (3) can be changed to:

$$\mathbf{U}(x, y) = \frac{1}{2\pi} e^{i\omega t} \int_{-\infty}^{\infty} \tilde{\mathbf{U}}(x, y)e^{i\beta z} d\beta, \tilde{\mathbf{U}}(x, y) = [\tilde{u}(x, y) \quad \tilde{v}(x, y) \quad \tilde{w}(x, y)]^T \quad (4)$$

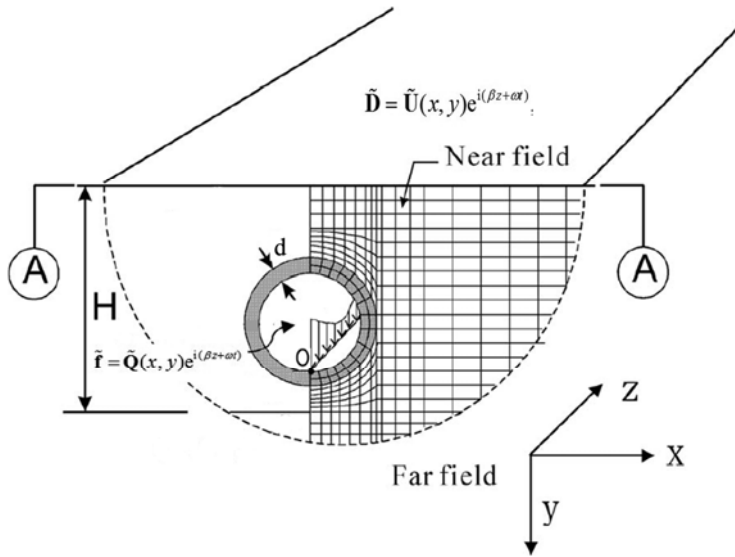


Figure 1: Schematical map of the periodic solution

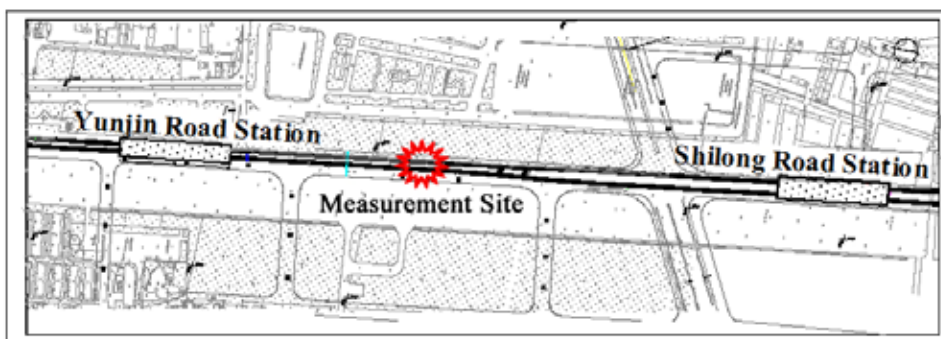


Figure 2: The route map of the monitored site (Shanghai metro line 11)

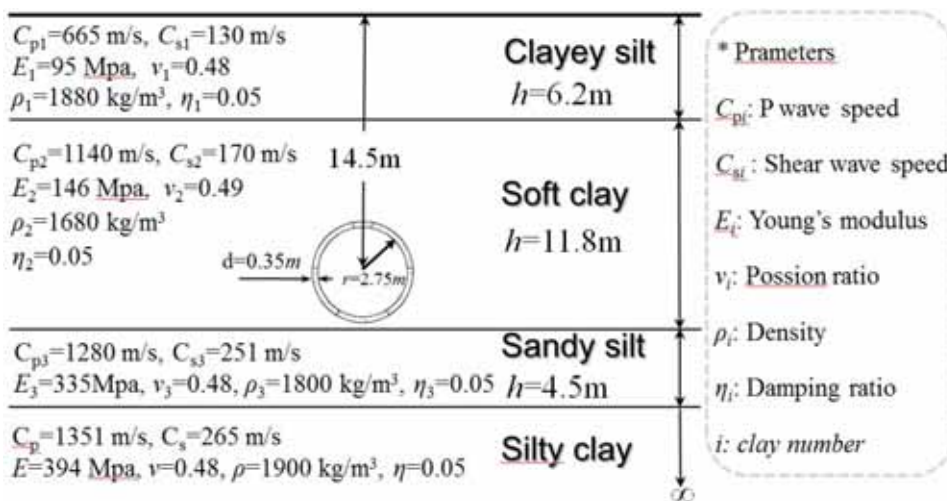


Figure 3: Parameters for the calculated cross-section

In the following analysis, such an approach is combined with the thin cylinder shell analytic theory and FE-IFE method, the expression will change accordingly. The details will be given in the following sections.

The field measurement was carried out at the section from Yunjin Road station to Shilong Road station of the Shanghai metro line 11. The route map is shown in Fig.2. The nearby area is an abandoned airport without large industry distribution. It has not been completed yet when the field measurement was performed. The vibration signal from the construction equipment would be found in the acquisition signals.

The cross-section of the tunnel has an internal radius $r=2.75$ m and a wall thickness $d=0.35$ m as shown in Fig.3. The tunnel lining is composed of six circumferential segments, which are connected by bolts in the circumferential and longitudinal direction of the tunnel. The concrete lining has a Young's modulus $E_l=35000$ MPa, a Poisson's ratio $\nu_l=0.25$, a density $\rho_l=2500$ kg/m³ and a hysteretic material damping ratio $\eta_l=0.02$. In this paper, only one tunnel is considered and its properties are assumed to be invariant in the longitudinal and circumferential directions.

As shown in Fig.3, the geological map of this area is obtained from a geological exploration report. It shows that there are mainly four types of soil layers: filling material and clayey silt, soft clay, sandy silt and silty clay. The dynamic soil characteristics are taken from a nearby large project exploration report presented in

Fig.3.

2.2 Dynamic characteristics of a free tunnel

Like conventional vibration-based SHM method, before analyzing the tunnel-soil coupled system, this section will first investigate the vibration characteristics of the free tunnel. Based on the parameters of the tunnel structure provided in the previous section, an analytic method combined with the periodic approach introduced by [Forrest and Hunt (2006); Hussein and Hunt (2007)] will be employed to search dispersion curves of the free tunnel. All the propagation modes appeared before 200Hz are plotted. Meanwhile, as a harmonic load with different frequency applied at the tunnel invert, it is found that the peaks of the driving point displacement FRFs match exactly with the tunnel in-plane propagation wave mode cut on frequency.

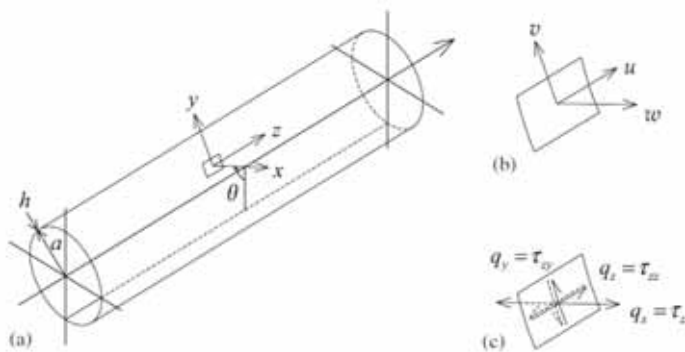


Figure 4: Schematic map used for the thin-walled cylindrical-shell theory

In practice, the tunnel can be analogous to an infinite extended hollow cylinder. As shown in Fig.4, [Flügge (1973)] describe the dynamic behavior of hollow cylinder using a thin cylinder shell. Then based on the periodic approach introduced in section 2, Forrest and Hunt further assumed that the applied loading and the motion of the shell are harmonic in the angular direction. Hence, the load and displacement component separable in time t , space z and angular position θ shown in Fig.4 has been expressed by Eq.(5) as [Forrest and Hunt (2006)]:

$$\begin{aligned}
 q_x(z,t) &= \tilde{Q}_{xn} \cos n\theta e^{i(\beta z + \omega t)}, & q_y(z,t) &= \tilde{Q}_{yn} \sin n\theta e^{i(\beta z + \omega t)}, \\
 q_z(z,t) &= \tilde{Q}_{zn} \cos n\theta e^{i(\beta z + \omega t)}, & u(z,t) &= \tilde{U}_n \cos n\theta e^{i(\beta z + \omega t)}, \\
 v(z,t) &= \tilde{V}_n \sin n\theta e^{i(\beta z + \omega t)}, & w(z,t) &= \tilde{W}_n \cos n\theta e^{i(\beta z + \omega t)}
 \end{aligned}
 \tag{5}$$

where, as shown in Fig.4, u , v and w are the displacement component, while q_x , q_y and q_z are the stress component. ω is angular frequency, β is wavenumber, and n is the wavenumber in the angular direction.

Substitution of the stresses and displacements from Eq.(5) into Flügge equations Forrest and Hunt (2006); Flügge (1973)], the motion of a thin cylindrical shell can be represented by a matrix form as Eq.(6)

$$[\mathbf{A}] \begin{Bmatrix} \tilde{U}_n \\ \tilde{V}_n \\ \tilde{W}_n \end{Bmatrix} = \frac{-a(1-\nu^2)}{Eh} \begin{Bmatrix} \tilde{Q}_{xn} \\ \tilde{Q}_{yn} \\ \tilde{Q}_{zn} \end{Bmatrix} \tag{6}$$

where $[\mathbf{A}]$ is a matrix of coefficients whose elements are given in Appendix A.1 of [Forrest and Hunt (2006)]. If loading $\mathbf{Q}_n = \{Q_{xn} \ Q_{yn} \ Q_{zn}\}^T$ is applied on the tunnel surface, the displacement FRFs $\mathbf{U}_n = \{U_n \ V_n \ W_n\}^T$ can be obtained in the wavenumber domain for a particular circumferential mode n . The actual stresses and displacements will be in general linear combinations of the individual modal quantities.

It is known that the dispersion curves are useful in investigating the mechanism of wave propagation in a medium, which are plotted as the wavenumber β of propagating modes versus the frequency ω , with the form $f = \Phi(\beta)$. Therefore, it is worth discussing the dispersion relation for waves in the free tunnel at first. There are different methods to calculate the dispersion curves [Metrikine and Vrouwenvelder (2000), Sheng, Jones and Thompson (2004)]. For non-zero solutions to exist, the determinant of the coefficient matrix of Eq. (6) must be equal to zero and expressed as:

$$\det(\mathbf{A}) = 0 \tag{7}$$

which is a function of frequency f and wavenumber β . The dispersion curves for every mode will be found by solving Eq.(3). An alternative way is to search the minimum of $|\det(\mathbf{A})|$. For this purpose, a matlab function is used and dispersion curves for every modes of free tunnel are plotted in Fig.5.

All modes for the range $n=0-5$ are presented in Fig.5, where $n=0$ corresponds to the first longitudinal compression wave and shear wave (torsional wave) mode, while $n=1$ corresponds to the first and second flexible wave mode of the cylinder. These three type modes will affect the wave propagation in the longitudinal direction mostly. Besides, the in-plane modes begin to appear as n increases. For $n=2-5$, four types of in-plane modes can be found.

As a radical unit loading applied on the inside surface of the free tunnel, the loading

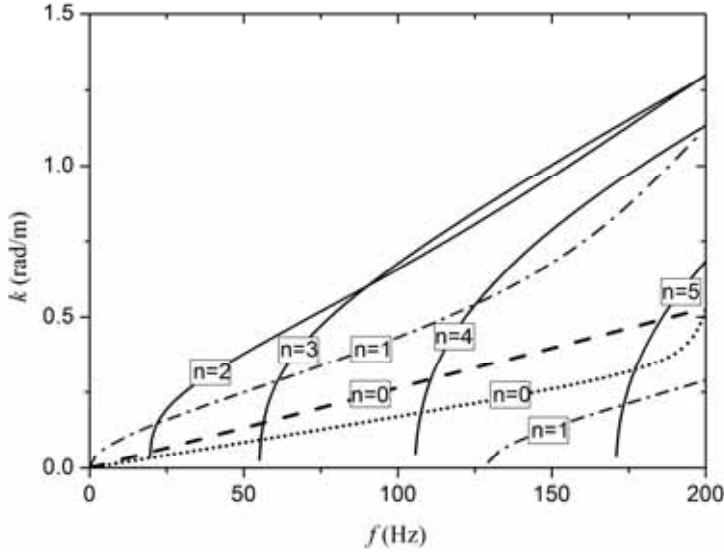


Figure 5: Dispersion curves of a free tunnel modeled as a thin-walled cylindrical shell

components \mathbf{Q}_n of Eq. (6) become

$$\tilde{\mathbf{Q}}_n = \begin{bmatrix} \tilde{Q}_{xn} \\ 0 \\ 0 \end{bmatrix} \begin{bmatrix} \cos n\theta & & \\ & \sin n\theta & \\ & & \cos n\theta \end{bmatrix}, \tilde{Q}_{xn} = \begin{cases} 1/2\pi a, & n=0 \\ 1/\pi a, & n \geq 1 \end{cases} \quad (8)$$

The FRFs in the radial direction at the driving point can be obtained as shown in Fig.6. It is found that the resonance frequencies of the free tunnel can be identified from the peaks of FRFs. It matches exactly with the cut on frequency of the first two ring modes ($n=2, 3$) as shown in Fig.5. As the resonance frequency varies with the tunnel parameters changes, such a dynamic characteristic is always used to vibration based defect detection. It is always used in detect the crack in the cylinder shell as reported by [Srinivasan and Kot(1998)], [Kim and Tse(2002)]., [Moore, Nichols and Murphy(2012)] further locate the crack position in a thin plate by combining Bayesian estimation. However, it will be found that all these characteristic disappeared as the cylinder coupled with soil.

2.3 Dynamic characteristics of the tunnel- soil coupled system

In this section, based on the approach of the 2.5D FE-IFE method, a Matlab toolbox is developed to compute the response of the tunnel-soil coupled system.

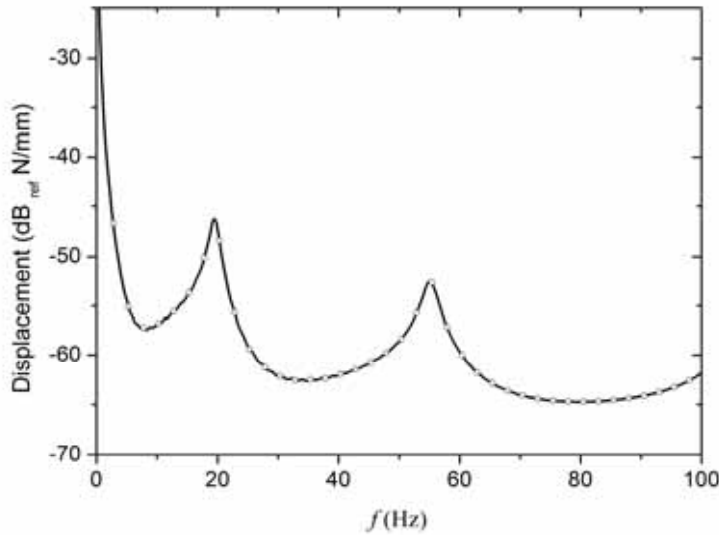


Figure 6: The driving-point response at the free tunnel invert

2.3.1 The 2.5D FE-IFE method

As shown in Fig.1, based on the periodic approach theory presented in section 2.1, one may simulate the whole system by only considering a profile perpendicular to the axis z , i.e., Profile A-A in Fig.1 which contains a near field of finite irregular region, and the boundary line represent for far field. In this study, the near field containing soils and tunnel structure is simulated by finite elements, where as the far field with unbounded soil is simulated by infinite elements. This approach has been addressed as 2.5D FE-IFE method by [Yang and Huang (2001, 2008)]. The approach will be introduced as follows.

According to Eqs.(1) and (2), for a harmonic load $\mathbf{Q}(x,y)e^{i(\beta z + \omega t)}$, the 3D time-history displacements of the system can be related to the displacements of the 2D profile as $\mathbf{U}(x,y)e^{i(\beta z + \omega t)}$. As shown in Fig.1, considering a vertical harmonic load with a self-oscillation frequency ω applied in the point O , the \mathbf{f} in Eq.(1) can be expressed as the Fourier transformation to equation $\mathbf{Q}=[0 \ 0 \ P(x,y)\delta(z)\exp(i\omega t)]^T$ and reads :

$$\tilde{\mathbf{Q}} = [0 \ 0 \ \tilde{Q}_z(x,y)]^T, \quad \tilde{Q}_z(x,y) = \frac{1}{2\pi} P(x,y) e^{i\omega t} \int_{-\infty}^{\infty} \delta(z) e^{i\beta z} dz = \frac{1}{2\pi} P(x,y) e^{i\omega t} \quad (9)$$

where $\delta(\cdot)$ is the Dirac delta function, $P(x,y)$ is the loading distribution function in $x-y$ plane. It follows that the originally three-dimensional continuous solid can

be discretized into elements in $x - y$ plane only. The displacements within each element can be interpolated as follows:

$$\tilde{u} = \sum_{i=1}^n N_i u_i, \tilde{v} = \sum_{i=1}^n N_i v_i, \tilde{w} = \sum_{i=1}^n N_i w_i \tag{10}$$

where N_i is the displacement shape function, n is the number of nodes for each element. The co-ordinates x and y within the element can be expressed as:

$$x = \sum_{i=1}^n M_i x_i, y = \sum_{i=1}^n M_i y_i \tag{11}$$

where M_i is the shape function for the co-ordinates, which represents the mapping of the element from the global coordinates $x - y$ to the local coordinates ζ and η . The shape functions N_i and M_i take different forms according to the different finite and infinite element types. For the finite element, the conventional Q8 plane element can be directly used, and N_i and M_i have the same form, n equals to 8. However for the infinite element, as given in [Yang and Huang (2001)], the shape function N_i and M_i have different forms. The details and parameters were also proposed in [Yang and Huang (2001)].

Substituting the displacement field expressed by Eq. (11) into the equation of virtual work, followed by discretization into a number of elements, the equation of motion in frequency domain can be written as:

$$([\mathbf{K}] - \omega^2 [\mathbf{M}]) \{\tilde{\mathbf{U}}\} = \{\tilde{\mathbf{Q}}\} \tag{12}$$

where $\{\mathbf{U}\}$ is the vector of nodal displacements, and $[\mathbf{K}]$ and $[\mathbf{M}]$ are the stiffness and mass matrices, $\{\mathbf{Q}\}$ denotes the vector of external loads. The expressions of the above matrix are expressed as:

$$\begin{aligned} [\mathbf{M}] &= \sum_e \rho \int_{-1}^1 \int_{-1}^1 N^T N |\mathbf{J}| d\eta d\zeta \\ [\mathbf{K}] &= \sum_e \int_{-1}^1 \int_{-1}^1 (B^* N)^T D (BN) |\mathbf{J}| d\eta d\zeta \quad \mathbf{J} = \begin{bmatrix} \sum_{i=1}^n \frac{\partial N_i}{\partial \eta} x_i & \sum_{i=1}^n \frac{\partial N_i}{\partial \eta} y_i \\ \sum_{i=1}^n \frac{\partial N_i}{\partial \zeta} x_i & \sum_{i=1}^n \frac{\partial N_i}{\partial \zeta} y_i \end{bmatrix} \\ \tilde{\mathbf{Q}} &= \sum_e \int_{-1}^1 \int_{-1}^1 N^T |\mathbf{J}| d\eta d\zeta \end{aligned} \tag{13}$$

where ρ is the mass density of the soil layer, $[\mathbf{J}]$ is the Jacobi function.

$$\mathbf{B} = \begin{bmatrix} \frac{\delta}{\delta x} & 0 & 0 & \frac{\delta}{\delta y} & 0 & -ik \\ 0 & \frac{\delta}{\delta x} & 0 & \frac{\delta}{\delta x} & -ik & 0 \\ 0 & 0 & -ik & 0 & \frac{\delta}{\delta y} & \frac{\delta}{\delta x} \end{bmatrix},$$

$$\mathbf{D} = \begin{bmatrix} \lambda' + 2\mu' & \lambda' & \lambda' & & & \\ & \lambda' + 2\mu' & \lambda' & & & \\ & & \lambda' + 2\mu' & & & \\ & & & \mu' & & \\ & & & & \mu' & \\ & & & & & \mu' \end{bmatrix}$$

where **[B]** is the stress-strain matrix and **[D]** is the material properties matrix. The parameters λ' , μ' are used, instead of Lamé's constants λ and μ , to describe the visco-elastic behavior of the considering soil and structure. The integration method for Eq. (13) is different for the finite element and infinite element method. The conventional Gauss integration is used for the finite element and an innovation method for the infinite element introduced in [Chow and Smith (1981)] is employed

2.3.2 Numerical implementation in MATLAB

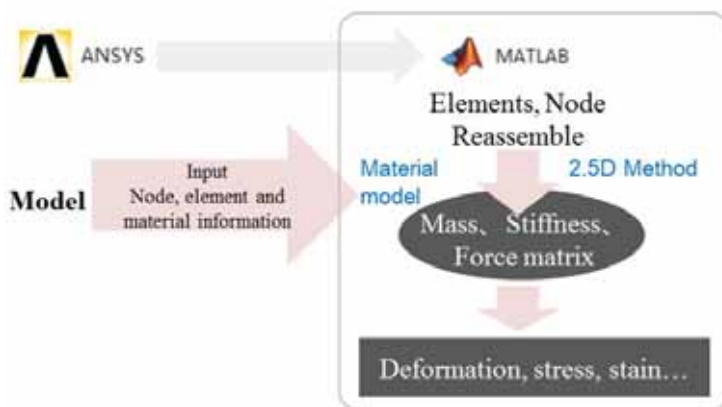


Figure 7: Flow chart for programming the 2.5D FE-IFE MATLAB toolbox

The above 2.5D FE-IFE method is developed in Matlab and a toolbox is developed. The steps are shown in Fig.7.

Step1: Built the considered model in ANSYS and export the node, element and material information into the MATLAB;

Step2: Based on the 2.5D FE-IFE method introduced in section 2.3.1, reassemble the global stiffness, mass and force matrix.

Step3: Solve Eq. (12) and export the stress and strain components in curves and clouds map.

2.3.3 The FRFs of tunnel-soil coupled system

Applying the toolbox introduced in section 2.3.2 to the problem of tunnels in Shanghai metro line 11, a tunnel embedded in the half space is considered in this section. The model mesh displayed in MATLAB is shown in Fig.8 where the tunnel and surrounding soil color in gray is modeled by the FEM, and the boundary color in white and dark around the finite element area is modeled by infinite element. The white one indicates that this boundary area is dominant by Rayleigh wave while dark one corresponds to P wave.

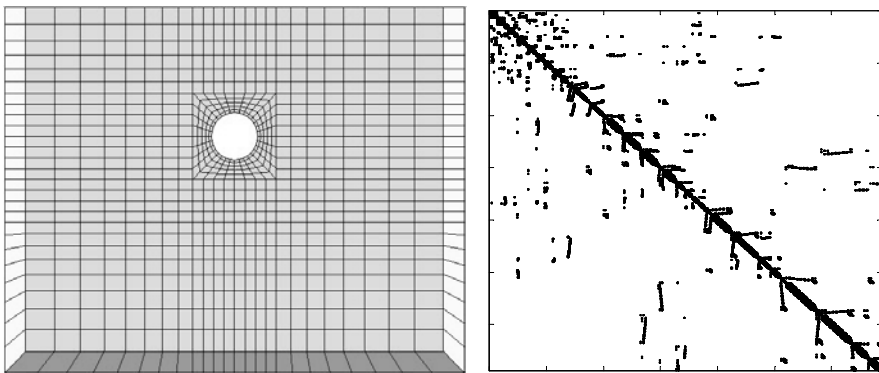


Figure 8: The modeling and global stiffness displayed in MATLAB

With a frequency increment of 0.25Hz, as the loading form in Eq.9 is applied at the tunnel invert in the above model to obtain the displacement FRFs as shown in Fig.9. It shows the displacement FRFs of the driving point response. By comparing with the displacement FRFs of the free tunnel, it is found that all the peak resonance frequency vanished and are replaced by the curves of amplitude slightly decreased, which is due to dynamic tunnel–soil interaction. Meanwhile, a new coupled resonance frequency of 1.5 Hz is found at the driving point FRFs.

3 Dispersion analysis and proposed SHM approach

The origin of the dynamic characteristics changes between free tunnel and tunnel-soil couple system will be explained by dispersion analysis in this section and a simple approach for SHM will be given based on the following analysis.

It is known that the coupled resonance frequency can be found by searching the intersection of the subsystem dispersion curves. To simplify analysis, a TTMM

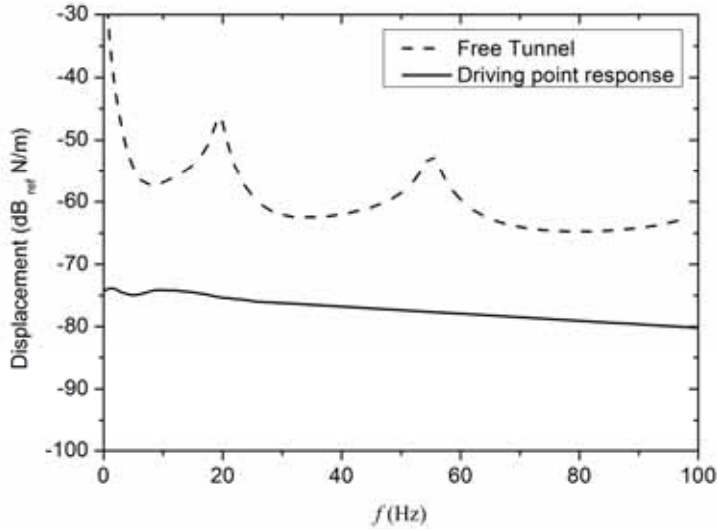


Figure 9: The differences of the driving-point displacement FRFs between the free tunnel and tunnel-soil couple system

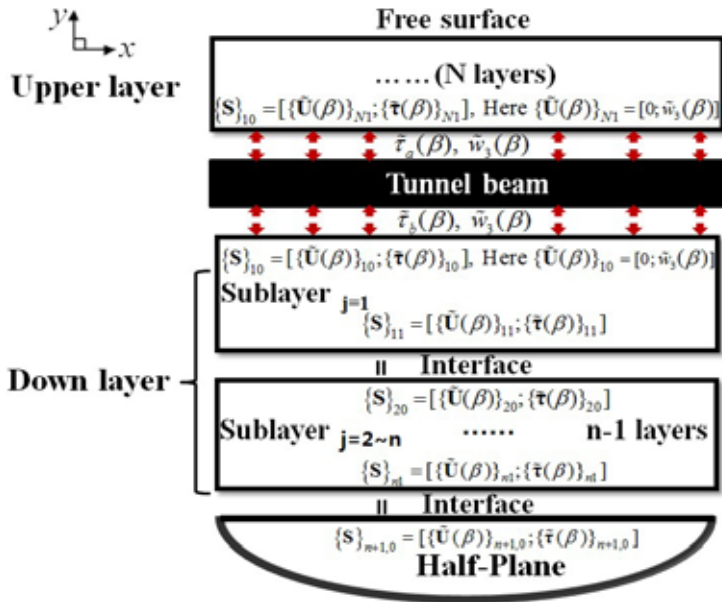


Figure 10: Schematic of model used for dispersion analysis

model is developed and employed for the dispersion analysis, where, the tunnel flexible wave mode is modelled by Timoshenko beam while the soil dispersion characteristics analysis is based on the transfer matrix method. With the previous analysis, the origin of the coupled resonance frequency is well explained and a novel approach is proposed to predict the tunnel structure Young’s modulus changes by means of the coupled resonance frequency in this section.

As shown in Fig.10, a 2D model consisting of two soil layers located above and beneath the tunnel is developed and employed in this section. The tunnel is modeled by Timoshenko beam while vibration propagation in soil layer is simulated by transfer matrix method. Thereby, it is termed as TTMM model. As mentioned above, in the condition that the equilibrium equations of force and displacement are established, dispersion curves can be obtained by searching the determinant of the coefficient matrix. Based on the transfer matrix method and according to the different boundary condition, the equilibrium equations between the force and displacement at the above and beneath tunnel beam-soil layer interface can be built. With transfer matrices for both the soil layer above and beneath the tunnel derived, the interaction between the tunnel beam and surrounding soil layers is determined. Therefore, the dispersion curves can be calculated.

3.1 Dispersion characteristics of the soil layer

3.1.1 Transfer matrix for the soil layer

The equation of motion for a single 2D soil layer with low viscosity can be written as [Kolsky, (1963)]:

$$\mu \nabla_{x,y}^2 \tilde{\mathbf{U}} + (\tilde{\lambda} + \tilde{\mu})(\nabla_{x,y} \nabla_{x,y} \tilde{\mathbf{U}}) = \rho \frac{\partial^2 \tilde{\mathbf{U}}}{\partial t^2}, \tilde{\mathbf{U}}(x,y) = \{\tilde{u}(x,y), \tilde{w}(x,y)\} \exp^{i\omega t} \quad (14)$$

where $\mathbf{U}(x,y)$ is the displacement vector as given in Eq.(2), ρ is the mass density of the soil layer, $\tilde{\lambda}$ and $\tilde{\mu}$ are operators used to describe the visco-elastic behaviour of the soil layer,

$$\tilde{\lambda} = \frac{\nu E(1 + i\eta)}{(1 + \nu)(1 - 2\nu)}; \tilde{\mu} = \frac{E(1 + i\eta)}{2(1 + \nu)}$$

Dividing each equation contained in Eq. (14) by ρ and summing gives

$$(\nabla^2 + k_1^2)\Psi(x,y) = 0; \Psi(x,z) = \frac{\partial \tilde{u}}{\partial x} + \frac{\partial \tilde{w}}{\partial y} \quad (15)$$

where $k_1 = \omega/c_1$, along with $c_1^2 = (\lambda + 2\mu)/\rho$. By applying the Fourier transformation to Eq. (15) with respect to x , Eq. (15) can be reduced to a simple differential

equation that represents the transform of the dilatation of the soil layer with the following solution:

$$\tilde{\Psi}(\gamma, y) = Ae^{-\alpha_1 y} + Be^{-\alpha_2 y} \tag{16}$$

where $\alpha_1^2 = \gamma^2 - k_1^2$. Substituting Eq. (16) into Eq.(15), the displacement at depth y of a specific soil layer j can be expressed as follows:

$$\begin{aligned} \tilde{\mathbf{U}}(\gamma, y) &= \begin{pmatrix} \tilde{u}(\gamma, y) \\ \tilde{w}(\gamma, y) \end{pmatrix} = \\ &= \frac{Ae^{-\alpha_1 y}}{k_1^2} \begin{pmatrix} -i\gamma \\ \alpha_1 \end{pmatrix} + \frac{Be^{\alpha_1 y}}{k_1^2} \begin{pmatrix} -i\gamma \\ -\alpha_1 \end{pmatrix} + Ce^{\alpha_2 y} \begin{pmatrix} 1 \\ -\frac{i\gamma}{\alpha_2} \end{pmatrix} + De^{-\alpha_2 y} \begin{pmatrix} 1 \\ \frac{i\gamma}{\alpha_2} \end{pmatrix} \end{aligned} \tag{17}$$

where A, B, C, D are constants. According to elasticity, the stress tensor can be obtained as:

$$\tilde{\tau}_{xy} = \mu(i\gamma\tilde{w} + \frac{d\tilde{u}}{dy}); \tilde{\tau}_{yy} = (\tilde{\lambda}\Delta + \frac{2\mu d\tilde{u}}{dy}) \tag{18}$$

The components of the stress tensor are thereby defined as:

$$\begin{aligned} \tilde{\boldsymbol{\tau}}(\beta, z) &= \begin{pmatrix} \tilde{\tau}_{xy}(\gamma, y) \\ \tilde{\tau}_{yy}(\gamma, y) \end{pmatrix} = Ae^{-\alpha_1 y} \begin{pmatrix} 2i\tilde{\mu}\alpha_1\gamma/k_1^2 \\ \tilde{\lambda} - 2\tilde{\mu}\alpha_1^2/k_1^2 \end{pmatrix} + Be^{\alpha_1 y} \begin{pmatrix} -2i\tilde{\mu}\alpha_1\gamma/k_1^2 \\ \tilde{\lambda} - 2\tilde{\mu}\alpha_1^2/k_1^2 \end{pmatrix} \\ &+ Ce^{\alpha_2 y} \begin{pmatrix} (\gamma^2 + \alpha_2^2)\tilde{\mu}/\alpha_2 \\ -2i\tilde{\mu}\gamma \end{pmatrix} + De^{-\alpha_2 y} \begin{pmatrix} -\tilde{\mu}(\gamma^2 + \alpha_2^2)/\alpha_2 \\ -2i\tilde{\mu}\gamma \end{pmatrix} \end{aligned} \tag{19}$$

Then, for the top interface of the j^{th} sublayer of a multilayer, where $y=0$, the displacement and stress vectors $\{\tilde{\mathbf{U}}(\gamma)\}_{j0}, \{\tilde{\boldsymbol{\tau}}(\gamma)\}_{j0}$ can be expressed in matrix form as:

$$\begin{aligned} \{\mathbf{S}\}_{j0} &= \begin{bmatrix} \{\tilde{\mathbf{U}}(\gamma)\}_{j0} \\ \{\tilde{\boldsymbol{\tau}}(\gamma)\}_{j0} \end{bmatrix} = [\tilde{u}(\gamma, 0); \tilde{w}(\gamma, 0); \tilde{\tau}_{xy}(\gamma, 0); \tilde{\tau}_{yy}(\gamma, 0)] = \mathbf{A}_{j0} \cdot \boldsymbol{\Theta} \\ \mathbf{A}_{j0} &= \begin{bmatrix} \frac{-i\gamma}{k_1^2} & \frac{-i\gamma}{k_1^2} & 1 & 1 \\ \frac{\alpha_1}{k_1^2} & \frac{-\alpha_1}{k_1^2} & \frac{-i\gamma}{\alpha_2} & \frac{i\gamma}{\alpha_2} \\ \frac{2i\tilde{\mu}\alpha_1\gamma}{k_1^2} & \frac{-2i\tilde{\mu}\alpha_1\gamma}{k_1^2} & \frac{\tilde{\mu}(\gamma^2 + \alpha_2^2)}{\alpha_2} & \frac{-\tilde{\mu}(\gamma^2 + \alpha_2^2)}{\alpha_2} \\ \tilde{\lambda} - \frac{2\tilde{\mu}\alpha_1^2}{k_1^2} & \tilde{\lambda} - \frac{2\tilde{\mu}\alpha_1^2}{k_1^2} & -2i\tilde{\mu}\gamma & -2i\tilde{\mu}\gamma \end{bmatrix}, \boldsymbol{\Theta} = \begin{bmatrix} A \\ B \\ C \\ D \end{bmatrix} \end{aligned} \tag{20}$$

In the same fashion, one can obtain the displacements and stresses, $\{\tilde{\mathbf{U}}(\gamma)\}_{j1}, \{\tilde{\boldsymbol{\tau}}(\gamma)\}_{j1}$, at the bottom of the j^{th} layer at depth y equal to h_j as:

$$\{\mathbf{S}\}_{j1} = \begin{bmatrix} \{\tilde{\mathbf{U}}(\gamma)\}_{j1} \\ \{\tilde{\boldsymbol{\tau}}(\gamma)\}_{j1} \end{bmatrix} = [\tilde{u}(\gamma, h_j); \tilde{w}(\gamma, h_j); \tilde{\tau}_{xy}(\gamma, h_j); \tilde{\tau}_{yy}(\gamma, h_j)] = \mathbf{A}_{j1} \cdot \boldsymbol{\Theta} \tag{21}$$

where

$$\mathbf{A}_{j1} = \mathbf{A}_{j0} \cdot \mathbf{D}_0; \mathbf{D}_0 = e^{\alpha_1 h_j} \begin{bmatrix} e^{-2\alpha_1 h_j} & & & \\ & 1 & & \\ & & e^{\alpha_2 h_j - \alpha_1 h_j} & \\ & & & e^{-\alpha_2 h_j - \alpha_1 h_j} \end{bmatrix}$$

where $\{\mathbf{S}\}_{j0}$ is the matrix representing the displacements and stresses at the top and $\{\mathbf{S}\}_{j1}$ is the one for the bottom of the j^{th} soil layer. Therefore,

$$\{\mathbf{S}\}_{j1} = \mathbf{A}_{j1} \cdot \mathbf{A}_{j0}^{-1} \{\mathbf{S}\}_{j0} = \mathbf{A}_{j0} \cdot \mathbf{D}_0 \cdot \mathbf{A}_{j0}^{-1} \{\mathbf{S}\}_{j0} \tag{22}$$

For multilayered soils, both the continuity conditions of displacements and stress should be satisfied at each interface between the sublayers [Haskell, (1953)]. The relationships are expressed by

$$\{\mathbf{S}\}_{11} = \{\mathbf{S}\}_{20}, \{\mathbf{S}\}_{21} = \{\mathbf{S}\}_{30}, \dots, \{\mathbf{S}\}_{n-1,1} = \{\mathbf{S}\}_{n,0} \tag{23}$$

Thus, according to Eqs.(22) and (23), for a multilayer with n sublayers, the relationship between the stresses and displacements at the top and bottom of the multilayer system can be written as [4] :

$$\{\mathbf{S}\}_{n1} = e^{\sum_{i=1}^n \alpha_i h_j} \mathbf{A}_{n1} \mathbf{A}_{n0}^{-1} \dots \mathbf{A}_{11} \mathbf{A}_{10}^{-1} \{\mathbf{S}\}_{10} = e^{\sum_{i=1}^n \alpha_i h_j} \begin{bmatrix} \mathbf{T}_{11} & \mathbf{T}_{12} \\ \mathbf{T}_{21} & \mathbf{T}_{22} \end{bmatrix} \{\mathbf{S}\}_{10} \tag{24}$$

Namely,

$$\begin{Bmatrix} \{\tilde{\mathbf{U}}(\gamma)\}_{n1} \\ \{\tilde{\boldsymbol{\tau}}(\gamma)\}_{n1} \end{Bmatrix} = e^{\sum_{i=1}^n \alpha_i h_j} \begin{bmatrix} \mathbf{T}_{11} & \mathbf{T}_{12} \\ \mathbf{T}_{21} & \mathbf{T}_{22} \end{bmatrix} \begin{Bmatrix} \{\tilde{\mathbf{U}}(\gamma)\}_{10} \\ \{\tilde{\boldsymbol{\tau}}(\gamma)\}_{10} \end{Bmatrix} \tag{25}$$

where \mathbf{T}_{11} , \mathbf{T}_{12} , \mathbf{T}_{21} , \mathbf{T}_{22} are 2×2 matrixes, $\{\tilde{\mathbf{U}}(\gamma)\}_{n1}$ and $\{\tilde{\boldsymbol{\tau}}(\gamma)\}_{n1}$ represent the stress and displacement vectors of the bottom interface of a multi-layer system, and $\{\tilde{\mathbf{U}}(\gamma)\}_{10}$ and $\{\tilde{\boldsymbol{\tau}}(\gamma)\}_{10}$ are the stress and displacement vectors for the top surface. In other words, the transmission of displacements and stresses through a layered soil system can be computed by solving the transfer matrix equation.

3.1.2 Dispersion equation

Using the transfer matrix in Eq. (25), the flexibility matrix for a layered soil system takes different forms, depending on the nature of the interfaces and boundary conditions. The stress and strain relationship at the beam and soil interface can

be determined once the specific boundary conditions are given. For the model depicted in Fig.1, two cases corresponding to the top and bottom interfaces of the beam can be described.

(1) The upside interface

As shown in Fig. 1, the soil layer above the track-tunnel coupled system is called the upper soil layer. The stress is equal to zero at the free surface, thus according to Eq. (25), $\{\tilde{\tau}(\gamma)\}_{10}$ can be treated as zero, $\{\tilde{\tau}(\gamma)\}_{N1}$ and $\{\tilde{\mathbf{U}}(\gamma)\}_{N1}$ correspond to the stress and displacement vectors at the interface of the tunnel and the upper soil layer, for which the relationship is

$$\{\tilde{\tau}(\gamma)\}_{N1} = \mathbf{T}_{21}\mathbf{T}_{11}^{-1}\{\tilde{\mathbf{U}}(\gamma)\}_{N1} = \mathbf{Q}_u\{\tilde{\mathbf{U}}(\gamma)\}_{N1} \tag{26}$$

When that the equilibrium equations between the force and displacement are established, as given in Eqs. (26), for non-trivial solutions to exist, the determinant of the coefficient matrix of the system should be equal to zero. Consequently, for the layered soils lying above the beam, the dispersion function can be expressed as:

$$\det(\mathbf{T}_{21}\mathbf{T}_{11}^{-1}) = 0 \tag{27}$$

(2) The downside interface

The half-spaced substratum beneath the tunnel comprises a soil layer called the down layer and a half-plane, as shown in Fig. 1. The stresses and displacements at $y=\infty$ can be considered to be zero. Thus, based on Eqs.(17) and (19), for a given depth y , the stress $\{\tilde{\tau}(\gamma, y)\}_{half}$ and displacement vectors $\{\tilde{\mathbf{U}}(\gamma, y)\}_{half}$ for the half plane can be written as:

$$\begin{aligned} \{\tilde{\mathbf{U}}(\gamma, z)\}_{half} &= \begin{pmatrix} \tilde{u}(\gamma, y) \\ \tilde{w}(\gamma, y) \end{pmatrix} = \frac{Be^{-\alpha_1 y}}{k_1^2} \begin{pmatrix} -i\gamma \\ \alpha_1 \end{pmatrix} + Ce^{-\alpha_2 y} \begin{pmatrix} 1 \\ i\gamma/\alpha_2 \end{pmatrix}; \\ \{\tilde{\tau}(\gamma, z)\}_{half} &= \begin{pmatrix} \tilde{\tau}_{xz}(\gamma, y) \\ \tilde{\tau}_{zz}(\gamma, y) \end{pmatrix} \\ &= Be^{-\alpha_1 y} \begin{pmatrix} 2i\tilde{\mu}\alpha_1\gamma \\ \lambda - 2\tilde{\mu}\alpha_1^2/k_1^2 \end{pmatrix} + Ce^{-\alpha_2 y} \begin{pmatrix} -\tilde{\mu}(\gamma^2 + \alpha_2^2)/\alpha_2 \\ -2i\tilde{\mu}\gamma \end{pmatrix} \end{aligned} \tag{28}$$

Further, one can calculate the stresses vector on the top of the half plane $\{\tilde{\tau}(\beta)\}_{n+1,0}$ in terms of the displacement vector $\{\tilde{\mathbf{U}}(\beta)\}_{n+1,0}$ as follows:

$$\begin{aligned} \{\tilde{\tau}(\gamma)\}_{n+1,0} &= \mathbf{MN}^{-1}\{\tilde{\mathbf{U}}(\gamma)\}_{n+1,0} = \\ & \begin{bmatrix} -2i\tilde{\mu}\alpha_1\gamma & \frac{\tilde{\mu}(\gamma^2 + \alpha_2^2)}{\alpha_2} \\ \tilde{\lambda} - \frac{2\tilde{\mu}\alpha_1^2}{k_1^2} & -2i\tilde{\mu}\beta \end{bmatrix} \begin{bmatrix} \frac{-i\gamma}{k_1^2} & 1 \\ \frac{-\alpha_1}{k_1^2} & \frac{-i\gamma}{\alpha_2} \end{bmatrix}^{-1} \{\tilde{\mathbf{U}}(\gamma)\}_{n+1,0} \end{aligned} \tag{29}$$

Herein, depending on the continuity of displacements and equilibrium of stresses between the down layer and the underlying half plane, the vectors $\{\tilde{\tau}(\gamma)\}_{n1}$ and $\{\mathbf{U}(\gamma)\}_{n1}$ in Eq. (25) can be replaced by $\{\tilde{\tau}(\beta)\}_{n+1,0}$ and $\{\mathbf{U}(\gamma)\}_{n+1,0}$ using Eq. (29). Thus, the stresses and displacements at the interface of the tunnel and the down layer, $\{\tilde{\tau}(\beta)\}_{10}$ and $\{\mathbf{U}(\gamma)\}_{1,0}$, can be related to each other as follows:

$$\begin{aligned} \{\tilde{\tau}(\gamma)\}_{10} &= \mathbf{R}^{-1}\mathbf{S}\{\tilde{\mathbf{U}}(\gamma)\}_{10} = \mathbf{Q}_L\{\tilde{\mathbf{U}}(\gamma)\}_{10} \\ \mathbf{R} &= \mathbf{T}_{22} - \mathbf{M}\mathbf{N}^{-1}\mathbf{T}_{12}; \mathbf{S} = \mathbf{M}\mathbf{N}^{-1}\mathbf{T}_{11} - \mathbf{T}_{21} \end{aligned} \tag{30}$$

Similar to Eq. (27), the dispersion equation for the layered soils lying beneath the beam can be expressed as:

$$\det(\mathbf{M}\mathbf{N}^{-1}\mathbf{T}_{21} - \mathbf{T}_{11}) = 0 \tag{31}$$

3.2 The dispersion relation between the free tunnel and surrounding soil

By solving the above Eqs (27) and (31) to obtain pure-real roots, the surrounding soil dispersion curves can be drawn. Only the soil layer beneath of the tunnel is considered because the site measurement is only implemented in the track and tunnel wall. As shown in Fig.3, the soil layer underneath the tunnel can be treated as a substrum consisting of a 4.5 m sandy silt layer and a silty clay half space, where the parameters are shown in Fig.3. The soil layer dispersion curves are plotted in Fig.11 and compared with the free tunnel dispersion curves (also shown in Fig.5).

From Fig.11, it is found that the first propagation wave mode of the soil layer is approximated as a straight line, the slope of which is equal to the Rayleigh wave speed for the soil layer beneath the tunnel. And it will only intersect with the tunnel flexible wave mode at 1.43Hz, as can be seen more clearly in Fig.13. The value is close to the simulation result given in Fig.9, indicating that the coupled resonance frequency corresponds to the intersection of the first propagation mode with the tunnel flexible wave mode.

3.3 The simplified approach for SHM

As described above, the coupled resonance frequency is induced by the intersection of the free tunnel flexible mode with the surrounding soil layer first propagation wave mode. And the dispersion curve of soil layer first propagation wave mode can be treated as a straight line at low frequency. Here it is also found that the free tunnel first flexible mode can be well modeled by a Timoshenko beam at the

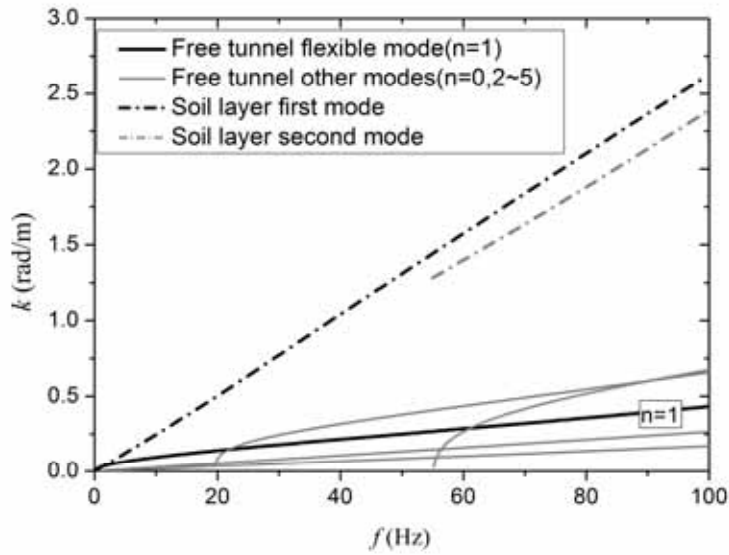


Figure 11: Dispersion curve of the soil layer beneath the tunnel beam

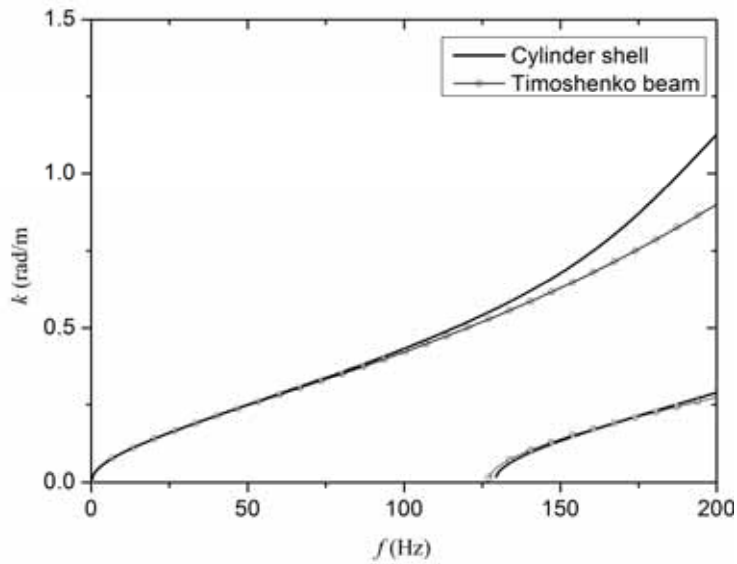


Figure 12: Comparison of the flexible modes propagating in thin cylindrical shell (n=1) and Timoshenko beam

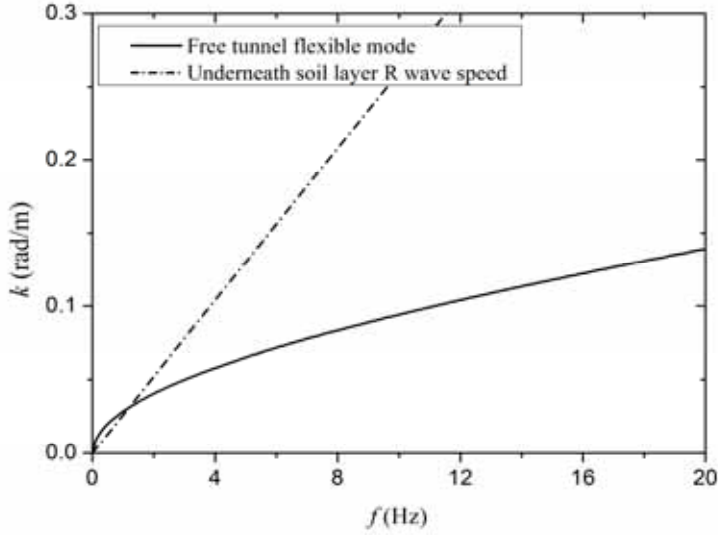


Figure 13: The dispersion relations of the free tunnel and underneath substructure

frequency ranging from 0 to 100Hz. In such a case, a formulation with respect to the tunnel Young’s modulus and the resonance frequency can be built. Therefore, the decrease of the tunnel global stiffness can be determined by changes of resonance frequency.

The motion equation of the Timoshenko beam can be expressed as:

$$\begin{aligned}
 E_t I_t \frac{\partial^4 w^4}{\partial x^4} + m_t \frac{\partial^2 w^2}{\partial t^2} - \left(\frac{E_t I_t m_t}{K A_c G} + \rho_t I_t \right) \frac{\partial^4 w^4}{\partial x^2 \partial t^2} + \frac{m_t \rho_t I_t}{K A_c G} \frac{\partial^4 w^4}{\partial t^4} \\
 = \left(1 + \frac{\rho_t I_t}{K A_c G} \frac{\partial^2}{\partial t^2} - \frac{E_t I_t m_t}{K A_c G} \frac{\partial^2}{\partial x^2} \right) p'
 \end{aligned}
 \tag{32}$$

Here w is the vertical motion of the Timoshenko beam, ρ_t is the density, E_t is Young’s modulus, I_t is the mass moment of inertia, and m_t is the mass per length, G is the shear modulus, A_c is the cross-sectional area of the tunnel beam.

The shear coefficient K is not a constant in the case of a thin hollow section [Hutchinson, 2001]. Therefore, a fit function against the wavenumber β is built to ensure that the dispersion curves can match the true solution. The expression obtained is:

$$K = 0.0342\beta^6 - 0.1621\beta^5 + 0.4155\beta^4 - 0.511\beta^3 + 0.1637\beta^2 - 0.0468\beta + 0.5799.$$

By applying two dimensional Fourier Transformation against time t and w to the

Timoshenko beam motion equation, and setting applied load p' equal to 0, the dispersion equation for the Timoshenko beam can be expressed as:

$$E_t I_t \beta^4 - m_t \omega^2 - \beta^2 \omega^2 \left(\frac{E_t I_t m_t}{K A_c G} + \rho_t I_t \right) + \omega^4 \frac{m_t \rho_t I_t}{K A_c G} = 0 \quad (33)$$

A Matlab function is coded to obtain the dispersion curves for the above Timoshenko beam in Fig.12. It is found that the dispersion curves of the Timoshenko beam match the first flexible wave modes of the cylindrical shell (corresponding to $n=1$) very well at the frequency ranging from 0 to 100Hz. The cut-on frequencies for the first and second flexible modes are 0 and 126Hz respectively. It is proved that the tunnel flexible mode can be modelled by Timoshenko beam very well in the frequency ranging from 0 to 100Hz.

By assuming the soil properties constant during the tunnel operation period and defining V_{soil} as the surrounding soil layer first propagation wave mode speed at low frequency (here it equal to the considering soil layer Rayleigh wave speed), as shown in Fig.13, in the intersection point of the free tunnel flexible mode and wave speed V_{soil} , the wavenumber β can be expressed by means of the resonance frequency ω_s and expressed as $\beta = \omega_s / V_{soil}$. Substitute it into Eq. (33) we obtain:

$$\left[E_t I_t - \left(\frac{E_t I_t m_t}{K A_c G} + \rho_t I_t \right) V_{soil}^2 + \frac{m_t \rho_t I_t}{K A_c G} V_{soil}^4 \right] \omega_s^2 - m_t V_{soil}^4 = 0 \quad (34)$$

The above equation is a formulation for the resonance frequency ω_s and tunnel material Young's modulus. With the other parameters considered as constant during the tunnel operation period, the variation of the resonance frequency ω_s corresponds to the alternation of the material Young's modulus. Thus, it is an index to judge the tunnel global stiffness.

4 Site measurement and validation

As an illustration example and to validate the simulation results given above, a site measurement has been carried out in the section from Yunjin Road to Shilong Road of Shanghai metro line 11 as shown in Fig.2.

The instrumentation plan for site measurements is shown in Fig.14. Every five of ten accelerometers are arranged in the tunnel wall and track with a spacing of 10m. The sensors arranged on the tunnel wall are LC130 while LC150A are arranged on the track. The details of the parameters for these two types of accelerometers are listed in Table 1. All the accelerometers are linked to a signal debug device and connected to the data acquisition device with synchronization.

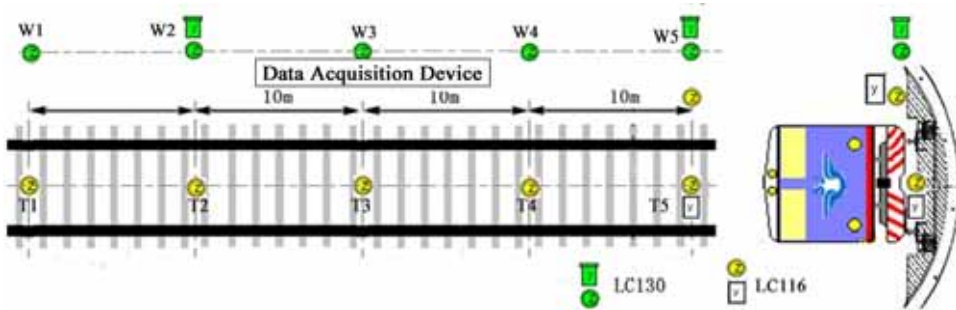


Figure 14: Arrangement map of the site measurement

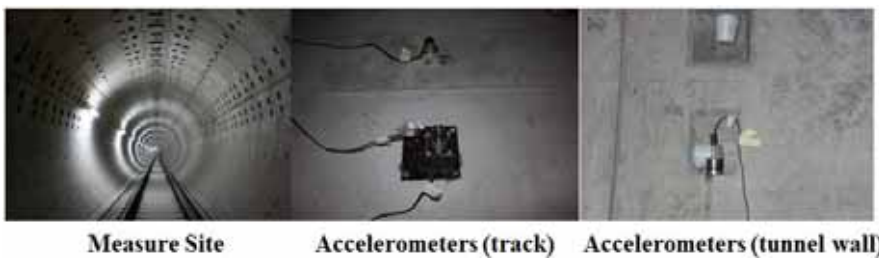


Figure 15: Pictures of the measurement site and accelerometers arrangement

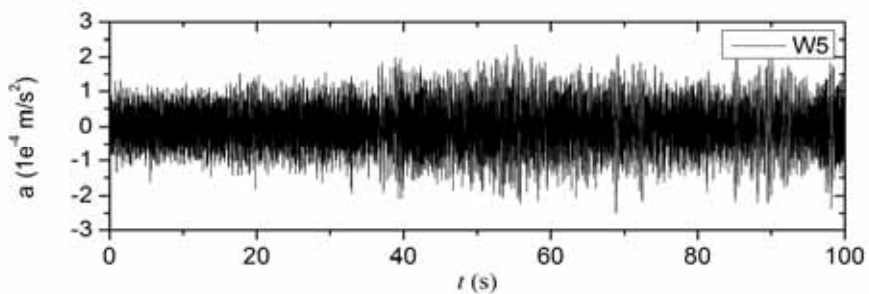


Figure 16: The time history of the white noise signal acquired at measure point W5

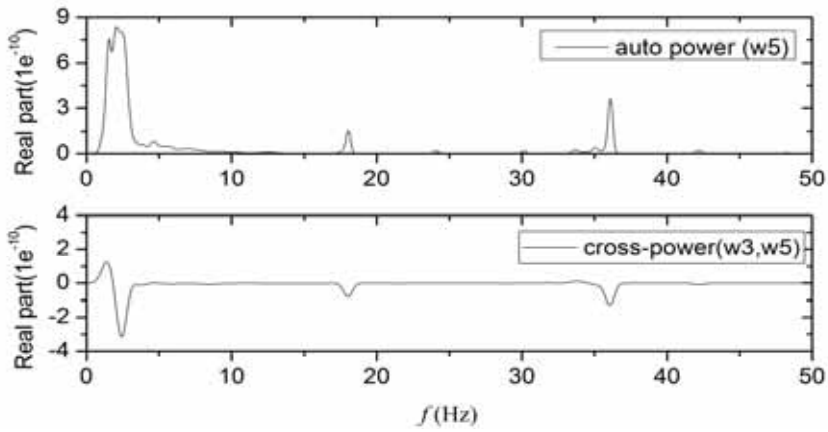


Figure 17: The auto/cross power spectrum of tunnel wall measure point

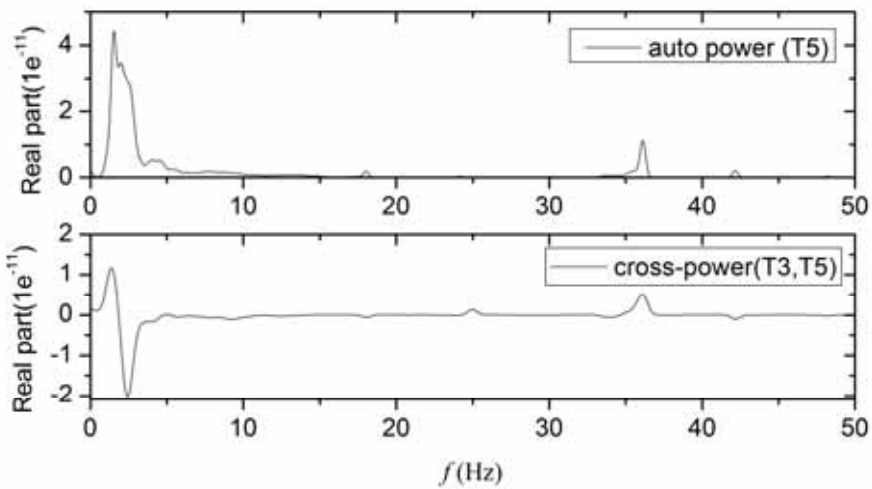


Figure 18: The auto/cross power spectrum of track measure points

Table 1: Parameters for the accelerometers

Sensor	Sensitivity (V/g)	Resolution (g)	Frequency range (Hz)	Max Acc. (g)
LC 130	40	5×10^{-7}	0.5-1000	0.12
LC 116	10	2×10^{-5}	0.1-300	0.5

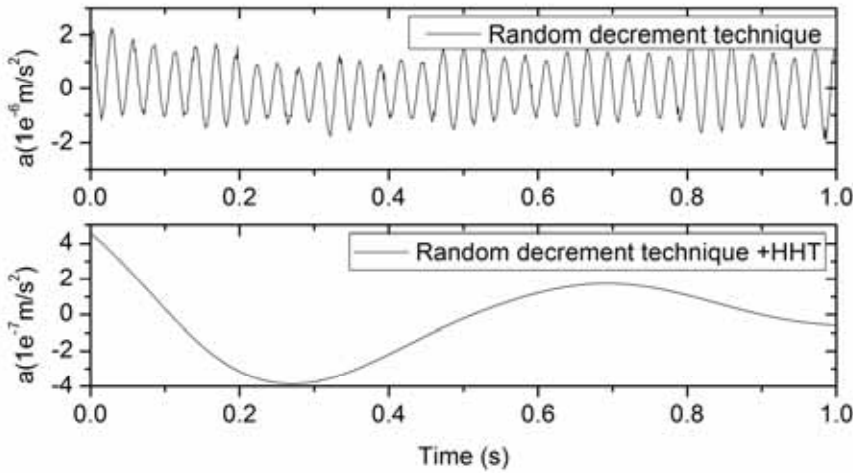


Figure 19: The mode shape corresponding to the coupled resonance frequency (W5)

The white noise signal acquired from the measure point W5 is shown in Fig.16, the total acquisition time is 1000s. During the time we carried out the site measurement, the construction in the Yunjin Road station has not completed yet. Therefore, the steady vibration excited by the construction machine would also be involved in the signal. If there is any resonance frequency of the tunnel-soil coupled system in this frequency range, it will be excited and identified from the auto-power and cross-power function spectrum of the measure points. Fig.17 and Fig.18 reveal that there is only one coupled resonance frequency. This validates the simulation results given in section 2.

From Fig.17, only one marked resonance frequency of 1.55Hz is found both in the auto-power function spectrum of W5 point and the cross-power function spectrum of the points W3 and W5 on the tunnel wall. Other two marked peaks exist with frequency of 18 and 36Hz; it is a multiple relationship and no phase flip has been found. Thus, it can be considered as noise from the construction work. From Fig.18, similar results can be found from the signals at the measure points T3 and

T5 on the track. The resonance frequency is equal to 1.5Hz, a little smaller than that on the tunnel wall.

Furthermore, random decrement technique is employed so as to extract the propagation wave mode corresponding to the 1.5Hz from the original signal. The result is shown at the top plot of Fig.19. And a non-attenuated wave type signal with a frequency of 36Hz is found. That provides further evidence that the peaks corresponding to 18Hz and 36Hz shown at Fig.17 and Fig.18 are not resonance frequency but the vibration signal induced by the construction machine. Meanwhile, the HHT [Huang (1971); Rilling, Flandrin and Goncalves (2003)] is employed to extract the couple mode shape and shown at the bottom of Fig.19.

Based on the above analysis, it is found that the coupled resonance frequency from site measurements agree well with the simulation results given in section 2.3.3 and dispersion analysis results supplied in section 3. The site measurement also validates the disappearance of the resonance frequency corresponding to the free tunnel ring-modes.

5 Conclusions

Taking the Shanghai metro line 11 as a cite study, the challenge of applying the conventional vibration-based SHM method to operation tunnel is discussed by exploring the vibration characteristics differences between free tunnel and tunnel-soil coupled system. By combining the periodic approach with an analytic method and the FE-IFE method, the simulation results reveal that any resonances frequency found from the free tunnel driving-point FRFs are lost when it coupled with soil layers, and meanwhile a coupled resonance frequency emerges at low frequency. The above simulation results are also validated by the site measurement. This indicates that it is difficult to use the conventional nature frequency and mode based SHM method in operational tunnel.

Based on a new developed model namely TTMM model, the origin of the dynamic characteristics changes between free tunnel and tunnel-soil coupled system is investigated by dispersion analysis. It is found that the coupled resonance frequency arise when the disperse curves of the free tunnel and soil layer intersect with each other. For the rest of frequency range, the FRFs become a smooth curve. In the present case, a tunnel buried in the soft clay, the coupled resonance frequency is 1.43Hz.

The above analysis shows that the disperse curve of the soil layer first propagation wave mode is approximated as a straight line with the slope equal to the considered underlying layer Rayleigh wave speed. Meanwhile, the first flexible wave mode existing in the free tunnel can be simulated by a Timoshenko beam. Therefore, by

assuming that the propagation wave speed of surrounding soil is determined and persisting during the tunnel operational period, a novel approach is developed to determine the relationship of the resonance frequency and Young's modulus built, which can be employed to judge the tunnel global stiffness and service condition.

Acknowledgement: The authors would like to acknowledge the financial support from the National Basic Research Program of China (973 Program: 2011CB013800), Shanghai Science and Technology Development Funds (12231200900, 11231201500), and the Program for Changjiang Scholars and Innovative Research Team in University (PCSIRT, IRT1029)

References

Aktan A.E.; Catbas F.N.; Grimmelsman K.A. (2003): *Development of a Model Health Monitoring Guide for Major Bridges*, Drexel Intelligent Infrastructure and Transportation Safety Institute.

Clouteau D.; Elhabre M. L.; Aubry D. (2000): Periodic BEM and FEM-BEM coupling-Application to seismic behaviour of very long structures, *Computational Mechanics*, Vol. 25, pp.567-577.

Carden E. P.; Fanning P. (2004): Vibration-based Condition Monitoring: A Review, *SHM(Structural Health Monitoring)*, Vol.3, pp. 355-377.

Chow Y.K; Smith I.M (1981): Static and periodic infinite solid elements, *International Journal for Numerical Methods in Engineering*, Vol. 17, pp.503-526.

Forrest J.A., Hunt H.E.M. (2006): A three-dimensional model for calculation of train-induced ground vibration, *Journal of Sound and Vibration*, Vol.294 (4-5), pp.678-705.

Forrest J.A., Hunt H.E.M (2006): Ground vibration generated by trains in underground tunnels, *Journal of Sound and Vibration*, Vol.294 (4-5), pp.706-736.

Flügge W. (1973): *Stresses in Shells*, second ed., Springer, Berlin.

Gupta S.; Degrande G.; Lombaert G. (2009): Experimental validation of a numerical model for subway induced vibrations, *Journal of sound and vibration*, Vol. 321 (3-5), pp.786-812.

Hutchinson J. R. (2001): Shear Coefficients for Timoshenko Beam Theory, *Journal of Applied Mechanics*, Vol. 68(1), pp.87-92.

Hussein M. F. M., Hunt H. E. M. (2007): A numerical model for calculating vibration from a railway tunnel embedded in a full-space, *Journal of Sound and Vibration*, Vol. 305, pp.401-431.

Haskell N. (1953): *Transmission of elastic waves through a stratified soil medium*,

Bulletin of the Seismological Society of America.

Huang N. E.; Shen Z.; Long S. R.; Wu M. C.; Shih H. H.; Zheng Q.; Yen N. C.; Tung C. C.; Liu H. H. (1971): The empirical mode decomposition and the Hilbert spectrum for nonlinear and non-stationary time series analysis, *Proc. R. Soc. Lond. A*, Vol. 454, pp. 903-995

Hwang R.N.; Lysmer J. (1981): Response of buried structures to traveling waves. *Journal of the Geotechnical Engineering*, Vol. 107(2), pp. 183-200.

Kolsky H. (1963) : *Stress waves in Solids*. New York Dover Publications.

Kim H.I.; Tse P. C. (2002): Locating damage in circular cylindrical composite shells based on frequency sensitivities and mode shapes, *European Journal of Mechanics-A/Solids*, Vol. 21(4), PP. 615–628.

Li J.P.; Wang R.L.; Yan J.Y. (2008): Research on structural status of operating tunnel of metro in Shanghai and treatment ideas, *Proceeding of the 6th International Symposium on Geotechnical Aspects of Underground Construction in Soft Ground*, pp.315-320.

Metrikine A.V.; Vrouwenvelder A. C. W. M. (2000): Surface ground vibration due to a moving train in a tunnel: two-dimensional model, *Journal of Sound and vibration*, Vol. 234(1), pp.43-66.

Moore E. Z.; Nichols J. M.; Murphy K. D. (2012): Model-based SHM: Demonstration of identification of a crack in a thin plate using free vibration data, *Mechanical Systems and Signal Processing*, Vol. 29, pp.284–295.

Peter C.C; Flatau A.; Liu S.C. (2003): Review Paper: Health Monitoring of Civil Infrastructure. *SHM(Structural Health Monitoring)*, Vol.2(3), pp.257-267.

Rilling G.; Flandrin P.; Goncalves P. (2003): On empirical mode decomposition and its algorithms, (*NSIP '03*)*Proceedings of the 6th IEEE/EURASIP Workshop on Nonlinear Signal and Image Processing*, Italy.

Srinivasan M.G.; Kot C.A. (1998): Damage index algorithm for a circular cylindrical shell, *Journal of Sound and Vibration*, Vol.215(3), pp. 587–591

Sheng X.; Jones C.J.C.; Thompson D.J. (2004): A theoretical study on the influence of the track on train-induced ground vibration, *Journal of Sound and Vibration*, Vol. 272 (3-5), pp.909–936.

Yang Y. B.; Hung H. H. (2001): A 2.5D finite/infinite element approach for modelling visco-elastic bodies subjected to moving loads, *International Journal for Numerical Methods in Engineering*, Vol.51, pp.1317-1336.

Yang Y. B.; Hung H. H. (2008): Soil vibrations caused by underground moving trains, *Journal of Geotechnical and Geoenvironmental Engineering*, Vol. 10, pp.1633-1644.